Dalton Transactions

Accepted Manuscript

ROYAL SOCIETY OF CHEMISTRY

www.rsc.org/dalton

Dalton Transactions

RSCPublishing

ARTICLE

Design, optical and antimicrobial properties of extremely thin alumina films colored with silver nanospecies†

Cite this: DOI: 10.1039/x0xx00000x

A. Jagminas,[a*] R. Žalnėravičius,[a] A. Rėza,[a] A. Paškevičius[b] and A. Selskienė[a],

Received 00th November 2014,
Accepted 00th November 2014

DOI: 10.1039/x0xx00000x

www.rsc.org/dalton

In this study, conditions for the fabrication of extremely thin and flexible anodic films decorated with silver nanowire arrays by alternating current treatments for the finishing of high purity and commercial aluminium foils were developed. For characterization of these porous films in thickness of ≤ 1.0 μm and encased silver species, inductively coupled plasma optical emission spectroscopy, X-ray diffraction and field emission scanning electron microscopy were used. Variable angle spectroscopic ellipsometry in the wavelength range of 200-1700 nm was also used to determine the influence of deposited Ag content and the film thickness on the optical constants (*n*, *k*) of the fabricated alumina films. It is shown that due to surprisingly low *k* values of nano-Ag-in-alumina films in the visible and near IR regions these films could be applied as transparent films with extremely low refractive index. In addition, the antimicrobial activity of the obtained films was assessed for the as-deposited and fully-encapsulated silver nanowire arrays against several wide-spread fungi and bacteria. The results obtained from *in vitro* tests indicated that as-formed Ag-in-alumina films containing ≥19 μg·cm^{-2} of silver possessed antimicrobial properties and could be promising as foodstuff package materials.

Introduction

Nanoscale materials frequently demonstrate unique physical and chemical properties due to their high surface area as well as quantum-sized effects.[1,2] In recent years, these effects have stimulated a rapid growth in studies devoted to fabrication of various nanostructured architectures and composites. Among others, silver nanoparticle-containing materials[3-5] and silver-based composites[6-11] with antimicrobial activity have been synthesized. These materials can reduce infections during burn treatment,[12,13] prevent bacteria colonization of dental materials,[14] catheters,[15,16] stainless steel instruments[17], textile products,[18,19] and human skin.[20,21] Note that silver nanoparticle-containing materials frequently demonstrate greater antimicrobial activity than silver ions alone, whose bactericidal properties have been known for centuries.[22] The smaller the Ag^0 particles are, the greater their ant imicrobial effects.[4,5,23] The bactericidal efficacy of silver-containing materials is frequently linked to the interaction of silver ions[24] or free radicals[25] with the liquid watery phase, resulting in membrane damage. As also reported, silver nanoparticles can exhibit genotoxic and cytotoxic effects in human tissues, causing DNA and cell damage if they are directly applied above a certain concentration.[26] However little is known about antibacterial and fungicidal properties of nm-scaled silver species encased inside the alumina pores although decoration processes of porous alumina films in thickness of ≥ 6.0 μm with nanowired silver arrays for the finishing of aluminium surface have been patented four decades ago.[27] It is worth also noting that usual anodic coatings are brittle and unsuitable for surface finishing of foodstuff package aluminium foils.

In this study, extremely thin porous alumina films were decorated in gold tints by alternating current deposition of silver in various contents and their antimicrobial activity against various microorganisms were tested. Variations in the ellipsometric parameters Ψ (psi) and Δ (delta) data with angle of incidence were also evaluated to determine the influence of deposited Ag content and film thickness on the optical constants (*n*, *k*) of the fabricated alumina films.

Experimental

Milli-Q water (18 MΩ) was used for preparation of all solutions. Aluminium (99.7 % purity) foil was purchased from

a State Research Institute Center for Physical Sciences and Technology, Institute of Chemistry, Gostauto 9, LT-01108 Vilnius, Lithuania. E-mail: jagmin@ktl.mii.lt
b Institute of Botany of Nature Research Centre, Zaliuju ezeru 49, LT-08406 Vilnius, Lithuania.

Electronic Supplementary Information (ESI) available: [details of any supplementary information available should be included here]. See DOI: 10.1039/b000000x/

Russia whereas high-purity foil in thickness of 0.127 mm (99.99 % purity) – from Sigma-Aldrich. The highest purity sulfuric, nitric and boric acids were purchsed from Labochem Ltd., and analytical grade $AgNO_3$, $MgSO_4$ and triethanolamine (TEA) from Sigma-Aldrich. *Saccharomyces cerevisiae*, *Micrococcus luteus*, *Escherichia coli*, *Aspergillus fumigatus*, and *Geotrichum candidum* cultures were obtained from the Botany institute of Nature Research Centre. For preparation of the *YEPD* medium, analytical grade peptone and galactose were purchased from Aldrich.

Aluminum samples, 40 mm × 40 mm × 0.05 mm, were cut from pure 50 μm thick, commercial Al foil (Al: 99.7%). The samples were chemically cleaned by etching in 1.5 mol·L^{-1} NaOH at ~ 60 °C for 15 s, rinsed for ~3 min with running water and desmutted for 60 s in a 1.5 mol·L^{-1} HNO_3 solution at ambient temperature. After careful rinsing in distilled water, the specimens were dried in a stream of Argon gas. The surface of high purity aluminium samples devoted to ellipsometric investigations was polished in the $HClO_4$-ethanol solution at 17 V and 7-10 °C.

Anodizing was carried out in a thermostated 15 ± 0.1 °C glass cell where aluminium foil was used as a working electrode and two platinum (45 mm × 70 mm × 0.5 mm) sheets were used as the counter electrodes. For anodizing an aqueous solution containing 1.2 mol·L^{-1} of H_2SO_4 was used. To obtain a thin and flexible porous film, the specimens were anodized at 15 ºC and 10 V for 10 min. For comparison, some specimens were anodized under the same conditions for 2 h, obtaining a porous alumina film with an average thickness of 9.5 μm. The as-anodized sample was rinsed with distilled water for 2 min and placed in the silver deposition bath containing 10 mmol·L^{-1} $AgNO_3$.

To obtain uniform deposition of silver within the extremely short alumina pores and uniform colouring of alumina film in gold tints, the composition of the electrolyte was modified by the addition of H_3BO_3, H_2SO_4, $MgSO_4$ and TEA. The counter-electrode was eight graphite strips connected together. Due to the rectifying properties of alumina barrier layer,[25] the depositions were carried out in alternating current (*ac*, 50 Hz) at either a constant effective *ac* current density or constant peak-to-peak voltage ($U_{p\text{-}to\text{-}p}$) modes. Anodized and coloured specimens were individually sealed in boiling distilled water for 10 min.

The content of deposited silver was determined by inductively coupled plasma optical emission spectroscopy analysis of solutions obtained *via* etching of 4.5 cm^2 Ag-in-alumina film in a hot HNO_3:H_2O (1:1) solution followed by careful rinsing and sonication in Milli-Q water. A high-resolution scanning electron microscope (SEM, Helios Nanolab 650) was used to examine the morphology of alumina films as well as the filling uniformity of alumina pores by the silver. For these observations, cross- sections of alumina films were obtained by cutting the film perpendicular to the substrate with a FIB focused Ga^+-ion beam.

Phase composition of coloured alumina films was studied by X-ray powder diffraction (XRD) using a D8 diffractometer (Bruker AXS, Germany), equipped with a Göbel mirror as a primary beam monochromator for CuK_α radiation. A step-scan mode was used in the 2Θ range from 30 to 80^o with a step-length of 0.02^o and a counting time of 8 s per step. The size of crystallites was determined from the broadening of all diffraction peaks using software PDXL and Halder-Wagner (H-W) approximation.

The optical properties of as-grown and decorated alumina films were investigated by means of spectroscopic ellipsometry in the wavelength range of 200-1700 nm by measuring the change in the polarization state (Ψ and Δ) of the light reflected off the surface of the film with an ellipsometer RC2. The Bruggeman Effective Medium Approximation (EMA) was applied to calculate the optical constants of mixed transparent Ag-in-alumina layer on aluminium substrate using the specified Cauchy dispersion, comprised of oxide, empty nanochannels and encased silver. The optical constants, e.g. refractive index *n* and extinction coefficient *k*, as well as the thickness of film *d* were evaluated by fitting the model functions to the measured data using CompleteEASE software program.

The antibacterial effects of the fabricated films were assessed by the *Saccharomyces cerevisiae* (*S. cerevisiae*) colony-forming unit assay (CFU) where Ag-in-alumina film pellets were incubated for various times in *YEPD* (1% yeast extract + 2% bacto peptone + 2% galactose) medium and the effects on colony-forming units analysed. An aqueous solution of methylene blue (0.01%) was applied for detection of killed yeast cells.

The antimicrobial activity of Ag-in-alumina samples against *Micrococcus luteus* SK4 (*M. luteus*), *Escherichia coli* SK 1.10 (*E. coli*), *Aspergilus fumigatus* BTL KO-5 (*A. fumigatus*), *Geotrichum candidum* BTL 2.1 (*G. candidum*) and *Candida parapsilosis* BTL C.7.2 (*C. parapsilosis*) was also investigated by the zone inhibition method. Following this method, the pieces of alumina films decorated with silver were pressed gently onto *Sabouraud CAF* agar or *Nutrient-agar* ("Liofilchem", Italy) plates inoculated with ≅10^6 CFU mL^{-1} microorganisms and analysed after 48 h incubation at 27±1 ºC.

All experiments were run in triplicate. Data from triplicate counts were averaged and the resulting values were applied for building corresponding diagrams.

Results

Fig. 1 shows surface and cross-sectional SEM images of alumina films fabricated by short-time (10 min) anodizing of aluminum at 10 V in 1.2 mol L^{-1} H_2SO_4 at 15 °C after *ac* treatment in a silver deposition bath. Images showed a porous anodic oxide film with an average pore diameter ($\varnothing_{pore}$) of 10 ± 0.5 nm and pore length of ~0.8 ± 0.1μm. SEM (*inset* in Fig. 1C) also revealed that the diameter and shape of the silver nanowires encased within the pores of such films by subsequent *ac* deposition were close to those of alumina pores. The mean size of the silver crystallites was 8 – 10 nm as assessed from the full width at a half maximum of the peaks *via* the Debye-Scherrer formulae. The deposition of silver at the bottoms of

tinny pores was observed from about 0.15 A dm^{-2}. The cross-sectional SEM observations also indicated that at 0.15 to 0.3 A dm^{-2} *ac* current density (j_{ac}) most of the alumina pores were filled to a height of ~200 – 250 nm. With further processing, an uneven growth of silver nanowires prevailed (Fig. 1D).

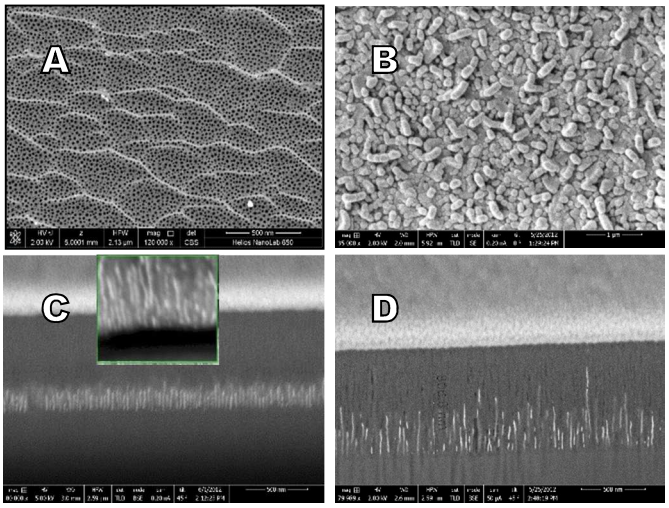

Fig. 1 Surface (A, B) and cross-sectional (C, D) SEM views of 0.8 μm thick porous alumina film after *ac* deposition of silver at a constant peak-to-peak voltage of 7.0 V mode for 600 (B), 40 (C) and 150 s (D).

Further *ac* treatments resulted in the deposition of silver onto the film surface (Fig. 1A) covering it with rod-shaped Ag^0 crystals (Fig. 1B). However, with precise control of the *ac* treatment conditions, a wide spectrum of uniform colours from light gold to bright brown could be obtained by this processing (*Inset* in Fig. 2).

From the XRD patterns (Fig. 2), the as-deposited silver nanowires within the alumina pores had a polycrystalline structure with the prevailing orientation along the [110] direction.

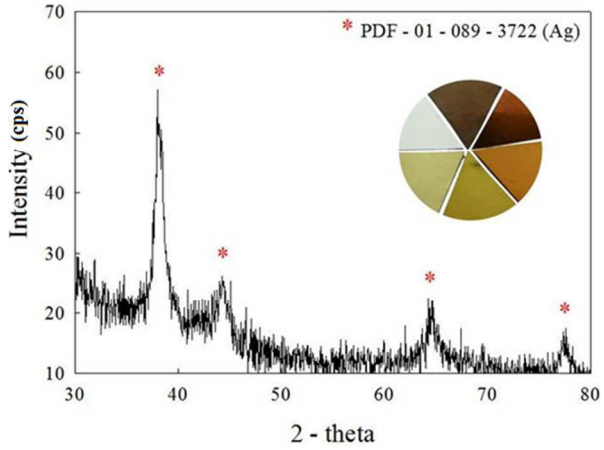

Fig.2 Typical XRD patterns of porous alumina film formed by anodizing of aluminum in 1.2 mol/L H_2SO_4 at 10 V and coloured *via* electrodeposition (*ac* treatments) of densely packed silver nanowires arrays. In the *inset* – the diagram of alumina colours can be obtained by this finishing method.

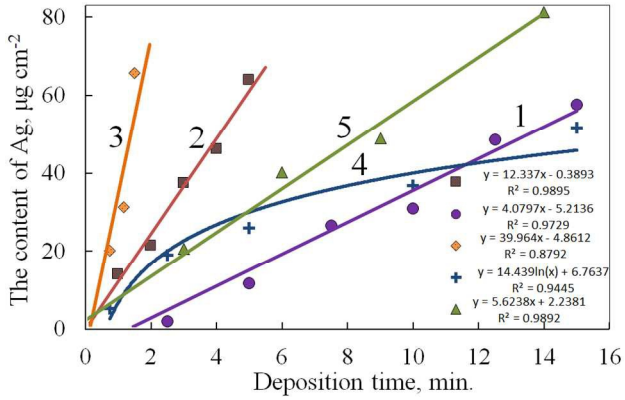

Fig. 3 Variations in the content of silver deposited inside the pores of alumina film from a solution containing 10 $AgNO_3$ and 50 mmol·L^{-1} $MgSO_4$ at a constant ac current density (A dm-2): 0.15 (1); 0.2 (2,5); 0.3 (3) and peak-to-peak voltage of 5.0 ± 0.3 V (4) with a processing time. Øpore≈ 10 nm and thickness of the alumina film (in μm) was: 0.8 (1-4) and 9.5 (5).

Quantitative results of silver deposition inside the pores of alumina film grown under study conditions in thickness of ≤ 1.0 μm are presented in Fig. 3. At a constant j_{ac} within the 0.15 to 0.3 A·dm^{-2} range, the deposition of silver inside the alumina pores proceeded at a constant rate strongly dependent on the j_{ac} value, while increasing the j_{ac} resulted in an increased silver deposition rate. It was interesting that at low current densities, the deposition started after some time possible required to re-construct the high-resistant barrier layer of alumina at the film oxide interface.[28] It was also surprising that deposition of silver inside the short, ca 0.8 μm, pores at a constant j_{ac} proceeded at a significantly higher rate (Fig. 3, plot 2) than in the pores of the same diameter in much thicker film (Fig. 3, plot 5).

Variability in the silver content deposited inside the pores of an extremely thin alumina film in constant *ac* voltage $U_{p\text{-}to\text{-}p}$ mode is shown in representative plot (4) of Fig. 3. As seen, in this case, the filling of alumina pores proceeded at a decreasing deposition rate which indicated that longer *ac* treatment times than at a constant current density are required for deposition of the same amount of silver. These data suggested that constant voltage *ac* regime was more suitable to achieving uniform colouring of alumina films in the same tint.

In this study, the optical constants (*n, k*) and the film thickness were determined by fitting the ellipsometric data (Ψ and Δ) using the specified Cauchy dispersion, comprised of aluminium oxide, empty nanochannels and silver nanowires (Fig. 4). Ten angles of incidence within 30° to 75° range with 5° step were used to obtain the dependencies of Ψ and Δ on the wavelength length (λ) at each angle (Fig. 5). It was determined that the variations of $\Psi(\lambda)$ and $\Delta(\lambda)$ at each angle calculated using the applied model match well with experimental both for pure (Fig. 6 a,b) and Ag-coloured (Fig. 6 c,d) films within the entire spectral interval. In this scenario, the optical constants for alumina samples were further evaluated for each angle of incidence within the tested wavelength range. Fig. 7a shows typical variations of $k(\lambda)$ and $n(\lambda)$ for alumina film of 900 ± 0.7 nm thickness grown under conditions of this study before and after deposition of ~8.0 μg silver, which colors it in gold.

Evidently, the variations of refractive index n and the extinction coefficient k with λ for pure alumina and the same alumina film decorated with silver nanowire array differ significantly; both $k(\lambda)$ and $n(\lambda)$ for Ag-in-alumina film show a sharp peak in a vicinity of 400-420 nm.

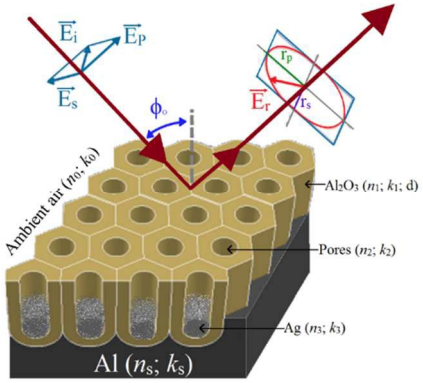

Fig. 4 The scheme corresponding to the model used for the fitting of experimental Ψ (λ) and Δ(λ) dependencies.

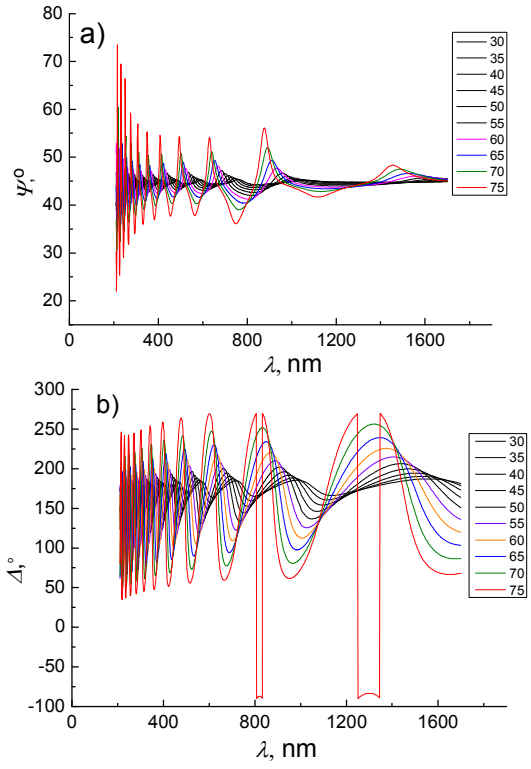

Fig. 5 The typical variations of ellipsometric parameters Ψ and Δ with wavelength λ at indicated angles of incidence for pure alumina film in thickness of 899.2 nm.

It is worth noting that increase in the content of deposited silver results in the increase of k and n values in this peak region (Fig. 8), whereas twofold increase in the alumina thickness leads to the approximately four times lower k and n values at each angle of incidence for the same content of encased silver.

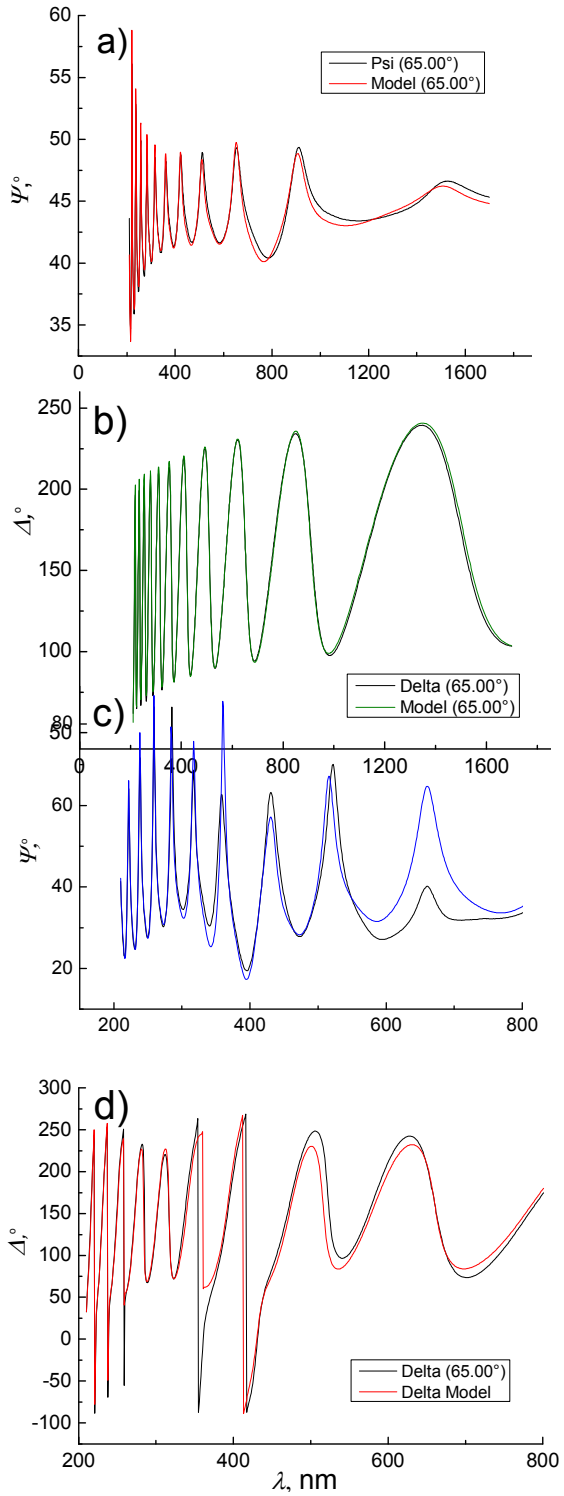

Fig. 6 Spectral ellipsometric data (ψ, Δ) of aluminium sample anodized in 1.2 mol L^{-1} H_2SO_4 at 15 °C and 10 V for 12 min (a,b) and then decorated with silver nanospecies by alternating current deposition at $U_{p\text{-}to\text{-}p}$ = 5.0 V for 30 s (c, d). The measurements were realized at an angle of incidence of 65^0. The curves in colour were calculated using the model system.

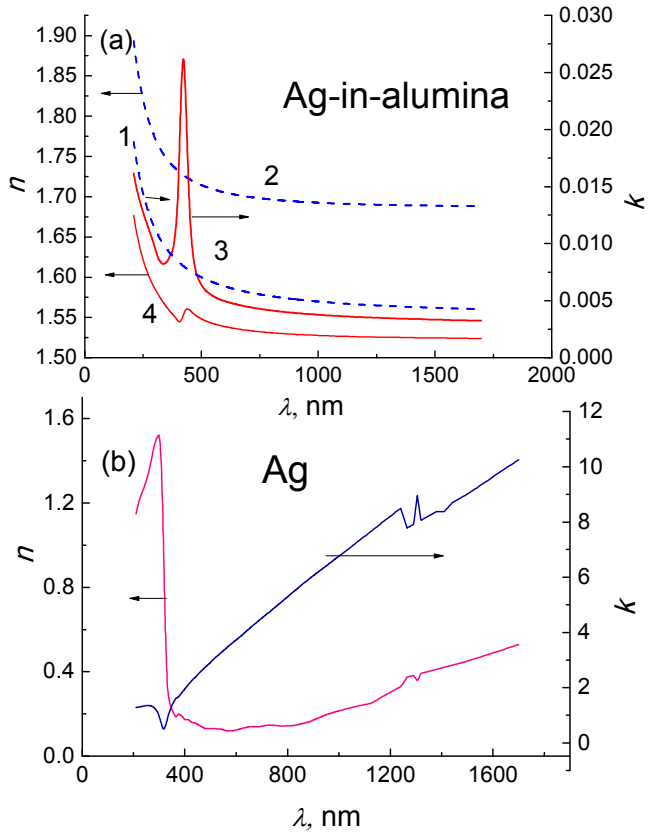

Fig. 7. (a): The spectral dependencies of the extinction coefficient *k* and the refractive index *n* of pure alumina film in thickness of 899.3 nm (1, 2) and a same film decorated with silver nanospecies in the content of 8.3 μg·cm^{-2} (3,4). Film roughness 5.09 nm. In (b) a same dependencies for bulk silver surface.

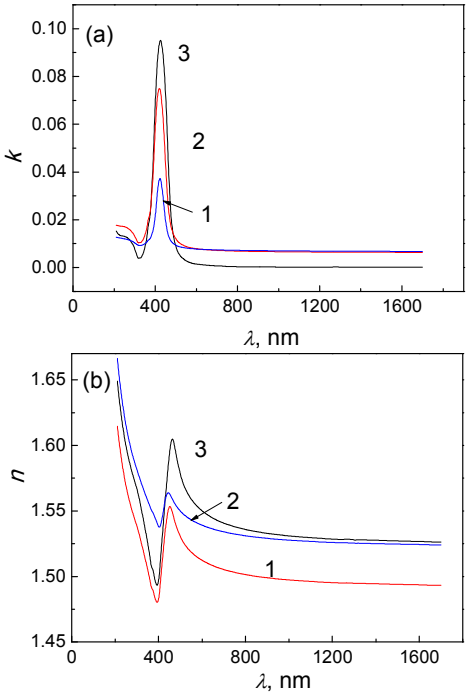

Fig. 8 The spectral dependencies of the extinction coefficient *k* (a) and the refractive index *n* (b) of alumina film decorated with silver nanospecies in contents: (1) 8.0; (2) 13.0 and (3) 15.0 μg cm^{-2}.

In order to evaluate the antimicrobial activity of silver nanowires encased inside the extremely thin alumina pores, *in vitro* tests were performed with *S. cerevisiae* colonization in *YEPD* medium with and without exposure to Ag-in-alumina pellets. Films sealed in boiling water and unsealed films containing defined amounts of deposited silver were investigated. For comparison, similar tests were performed by incubation of yeast cells (*S. cerevisiae*) in YEPD medium containing 1.0, 2.5, and 5.0 ppm Ag^+ ions, pure alumina film, and silver-coated alumina film pellets. The results obtained from these antimicrobial activity assays against *S. cerevisiae* are shown in Fig. 9.

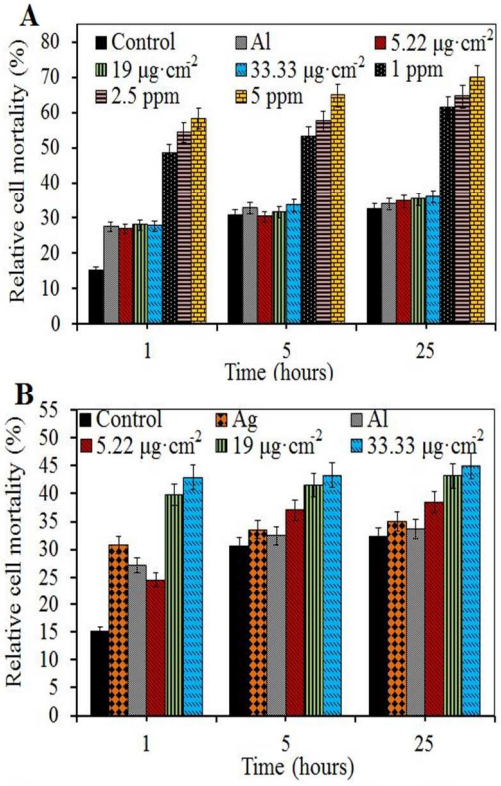

Fig. 9 Percentage of dead *S. cerevisiae* cultured in *YEPD* medium in the absence and presence of various as-grown (B) and sealed (A) Ag-in-alumina samples (silver contents indicated) after 1, 5, and 25 h incubation. Error bars represent standard deviation.

It is seen that when the silver was fully encapsulated inside the alumina pores, fungicidal activity was insignificant and independent of the content of encased silver (Fig. 9A) which could be explained by the slow release and diffusion of Ag^+ ions through the surface layer of the sealed alumina film. For unsealed Ag-in-alumina films (Fig. 9B), the silver content contributed to the fungicidal effect. It is also interesting to note that nanowired Ag^0 species had a higher inhibitory activity towards *S. cerevisiae* than silver-coated alumina film. These results are corroborated by other studies which indicate that the antimicrobial activity of nanostructured particles, such as Fe_3O_4,[29] ZnO,[30] MgO[31], and Ag^0,[4,5,23] increased with decreasing particle size.

Antimicrobial activity of Ag-in-alumina samples was also investigated by the zone inhibition method. Following this method, pieces (~1.5 cm^2) of alumina decorated with silver nanowire arrays were pressed gently onto the surface of agar plates, incubated with 10^6 CFU mL^{-1} of uniformly dispersed bacteria, yeast or fungi, and analyzed after 5, 10 and 48 h incubation at 27 ºC. We note that most of the tested microorganisms are prevailing in the human's nitty-gritty. Table 1 display the representative zones inhibition for Ag-in-alumina samples in the *A. fumigatus* plates and the $AgNO_3$ (100 µL) solutions. These results suggested that all Ag^+ solutions tested had a fungicidal influence effect at some distance from the drop centre. For the as-deposited Ag-in-alumina samples tested against *A. fumigatus*, a wide zone of inhibition could be seen for films containing ≥19 µg·cm^{-2} of silver, suggesting fungi-static activity for the silver nanowires encased inside the thin alumina pores. A similar effect was seen against *G. candidum* (Table 1) but not *C. parapsilosis*.

No fungistatic activity was seen for sealed (boiling in water) Ag-in-alumina films against all fungi tested. This effect could be attributed to the lack of direct contact between fungi and silver molecules, as well as decreased content of the silver ions diffusing through the compact alumina surface layer.

In the next setup, Ag-in-alumina specimens containing various silver contents were tested against gram negative (*E. coli*) and gram positive (*M. luteus*) organisms in Mueller-Hinton Agar by the standard well diffusion method[32] and the results are presented in Table 2. Data indicated that Ag-in-alumina films containing ≥19 µg cm^{-2} of silver exhibited antimicrobial properties against both bacterial species. However, the zone of inhibition around as-grown Ag-in-alumina samples was ~90 % wider for the gram-negative *E. coli* than for the gram-positive *M. luteus*. This behavior is similar to previously reported data where a significantly higher bactericidal activity was seen for silver nanocomposite materials against gram-negative bacteria,[33] attributed to differing structures of their cell walls.

Discussion

Aluminium foils as nontoxic and quite inexpensive materials have been used for decades for packaging of sweets and chocolates. Chemical stability of aluminium is linked to spontaneous oxidation of this metal at the damaged places even at ambient conditions. To increase chemical stability, the thickness of naturally formed Al oxide can simply be increased by thermal, chemical or electrochemical oxidation. In fact, the short-time anodizing of Al in aqueous solutions of sulfuric acid at lower bath concentrations and voltages, ca 1.2 M and 10 V, respectively, instead of typical 1.8 - 2.0 M and 17 - 18 V, have been chosen in this study in order to form nanoporous oxide layer with thickness less than 1.0 µm . We note that such films contained approximately (1.5 - 1.7)×10^{11} pores cm^{-2}, densely packed and oriented perpendicularly to the substrate, while still retaining elasticity, which is particularly crucial for packaging material. It is also noteworthy that decrease in the anodizing voltage down to 10 V resulted in the formation of thinner barrier layer at the alumina film | Al interface. We report that this circumstance allowed us to uniformly deposit silver inside the short (< 1.0 µm) and tinny ($Ø_{pore}$≤10 nm) channels by AC treatment. To the best of our knowledge, this is the first demonstration of uniform coloring of extremely thin alumina films by electrochemical approach. The first reason for deposition of silver inside the alumina pores was the fact that only nm-scaled Ag species dispersed uniformly in the clear matrices even in the contents of less than 0.1 g·m^{-2} color them in esthetic gold tints. Besides, we expected that densely packed silver nanowires, as small as ~10 nm in diameter and 50 - 200 nm in length, encased in porous alumina films, as thin as ≤ 1.0 µm, could exhibit antimicrobial activity even after full encapsulation of Ag species. On the other hand, it is also likely that silver will not be able to penetrate through the layer of aluminium oxide formed at the top-side during sealing in boiling water. Therefore, the antibacterial as well as antifungal activities of Ag-in-alumina films, both sealed and unsealed, were studied herein using several wide-spread microorganisms including *S. cerevisiae, M. luteus, E. coli, A. fumigatus, G. candidum, and C. parapsilosis*. Our results indicated that in contrast to unsealed alumina, fully encapsulated silver species had significantly weaker or none antimicrobial effects most likely due to the absence of direct contact between microorganisms and Ag species. The results of the present study are in agreement with other reports that indicate greater activity of silver nanoparticles against gram-negative microorganisms.[33]

It was also determined that optical parameters of alumina film changed significantly after deposition of silver at the bottom part of alumina pores. Both $k(\lambda)$ and $n(\lambda)$ for Ag-in-alumina film show a sharp peak in a vicinity of 400 - 420 nm. The height of these peaks is related with the content of deposited silver. Increase in the content of deposited silver results in the increase of k and n parameter values in this peak region. Surprisingly low dispersion extinction coefficient k of Ag-in-alumina films in wavelength range of 500 - 1700 nm, e.g. 0.004 - 0.0015 and $dk/d\lambda = l\text{-}2\cdot10^{-6}$ 1/nm, with respect to those of the bulk silver, where $k \cong 2.0$ - 10.0 and $dk/d\lambda = 6\cdot10^{-3}$ 1/nm, (see Fig. 7b) imply on the prospective applications of alumina films decorated with silver nanospecies in the optoelectronic devices for fabrication of transparent films with low refractive index.

Conclusions

In this study, conditions were established for finishing aluminium foils in uniform gold-tints *via* formation of a thin (<1 µm) porous anodic film and the subsequent *ac* deposition of silver nanowire arrays. The antimicrobial properties of as-grown and sealed Ag-in-alumina films were tested *in-vitro* against several fungi, bacteria, and yeast. Results indicated that as-deposited Ag-in-alumina films, in contrast to fully encapsulated Ag-in-alumina films, possessed antimicrobial activity against most of the organisms tested in this study, suggesting the potential use in aluminium foils finishing and foodstuff packaging materials.

Variations of the optical parameters, e.g. the refractive index n and the extinction coefficient k, with λ of Ag-in-alumina film demonstrate the sharp peaks in the vicinity of 400-420 nm contrary to the pure film. The height of these peaks is related with the content of deposited silver and increases with loading. Extremely low k values of nano-Ag-in-alumina films in the visible and near IR regions within the λ range from 500 to 1700 nm suggest the possible application of these films in fabrication of transparent films with low refractive index.

Notes and references

1 A. Huczko, *Appl. Phys.*, 2000, **70**, 365-376.
2 X. Battle, A.J. Labarta, *Appl. Phys.*, 2002, **35**, 15-42.
3 I. Sondi, B. Salopek-Sondi, *J. Coll, Interf. Sci.*, 2004, **275**, 177-182.
4 J.R. Morones, J.L. Elechiguerra, A. Camacho, K. Holt, J.B. Kouri, J.T. Ramirez, M.J. Yacaman, *Nanotechnology*, 2005, **16**, 2346-2353.
5 C. Baker, A. Pradhan, L. Pakstis, D.J. Pochan, S.I. Shah, J. *Nanosci. Nanotech*., 2005, **5**, 244-249.
6 L.Z. Zhang, J.C. Yu, H.Y. Yip, Q. Li, K.W. Kwong, A.W. Xu, P.K. Wong, *Langmuir*, 2003, **19**, 10372-10380.
7 Z. Zheng, W. Yin, J.N. Zara, W. Ji, J. Kwak, R. Mamidi, et al. *Biomaterials*, 2010, **31**, 9293-9300.
8 D. Lee, R.E. Cohen, M.F. Rubner, *Langmuir*, 2005, **21**, 9651-9659.
9 P.L. Taylor, A.L. Ussher, R.E. Burrell, *Biomaterials*, 2005, **26**, 7221-7229.
10 S.P. Chen, G.Z. Wu, H.Y. Zeng, *Carbohydr. Polym.*, 2005, **60**, 33-38.
11 S. Shanmugam, B. Viswanathan, T.K. Varadarajan, *Mater. Chem. Phys*., 2006, **95**, 51-55.
12 E. Ulkur, O. Oncul, H. Karagoz, E. Yeniz, B. Celikoz, *Burns*, 2005, **31**, 874-877.
13 D.V. Parikh, T. Fink, K. Rajasekharan, N.D. Sachinvala, A.P.S. Sawhney, T.A. Calamari, A.D. Parikh, *J. Text. Res*., 2005, **75**, 134-138.
14 S. Ohashi, S. Saku, K. Yamamoto, *J. Oral Rehabil*., 2004, **31**, 364-367.
15 M.E. Rupp, T. Fitzgerald, N. Marion, V. Helget, S. Puumala, J.R. Anderson, P.D. Fey, *Am. J. Infect. Contr.*, 2004, **32**, 445-450.
16 U. Samuel, J.P. Guggenbichler, *Intern. J. Antimicrob. Agents*, 2004, **23**, 75-78.
17 M. Bosetti, A. Masse, E. Tobin, M. Cannas, *Biomaterials*, 2002, **23**, 887-892.
18 T. Yuranova, A.G. Rincon, A. Bozzi, S. Parra, C. Pulgarin, P. Albers, J. Kiwi, *J. Photochem. Photobiol*., 2003, **161**, 27-34.
19 S.H. Jeong, S.Y. Yeo, S.C. Yi, *J. Mater. Sci*., 2005, **40**, 5407-5411.
20 A. Gauger, M. Mempel, A. Schekatz, T. Schafer, J. Ring, D. Abeck, *Dermatology*, 2003, **207**, 15-21.
21 H.J. Lee, S.H. Jeong, *Text. Res. J*., 2005, **75**, 551-556.
22 D. Wei, W. Sun, W. Qian, Y. Ye, X. Ma, *Carbohydr. Res*., 2009, **344**, 2378-2382.
23 A. Panaček, L. Kvitek, R. Prucek, M. Kolar, R. Večerova, N. Pizurova, et al., *J. Phys. Chem*., 2006, **110**, 16248-16253.
24 R. Kumar, A. Münstedt, *Polymer Internat*., 2005, **54**, 1180-1186.
25 J.S. Kim, E. Kuk, K.N. Yu, J.-H. Kim, S.J. Park, H.J. Lee, et al., *Nanomed. Nanotechn. Biol. Med.*, 2007, **3**, 95-101.
26 I. Papageorgiou, C. Brown, R. Schins, et al., *Biomaterials*, 2007, **28**, 2946-2958.
27 E.Herrmann, *Galvanotechnik*, 1971, **62**, 867-901.
28 A. Jagminienė, G. Valinčius, A. Riaukaitė, A. Jagminas, *J. Crys. Growth*, 2005, **247**, 622-631.
29 N. Tran, A. Mir, D. Mallik, A. Sinha, S. Nayar, T. Webster, *Int. J. Nanomed*., 2010, **5**, 277-283.
30 O. Yamamoto, et al., *Carbon*, 2001, **39**, 1643-1651.
31 S. Makhluf, R. Dror, Y. Nitzan, Y. Abramovich, R. Jelinek, A.Gedanken, *Adv. Funct. Mater*., 2005, **15**, 1708-1715.
32 R. Thomas, A. Viswan, J. Mathew, R. Ek, *Nano Biomed. Eng*., 2012, **4**, 139-143.
33 S. Egger, R.P. Lehmann, M.J. Height, M.J. Loessner, M. Schuppler, *Appl. Environ. Microbiol*., 2009, **75**, 2973-2976.

Table 1 The results of fungi growth inhibition by as-deposited silver nanowire arrays in alumina pores and Ag+ ions.

Culture	Contacting materials	The content of Ag^o in μg or [Ag+]	Effect	Zone of inhibition (in mm)
A. fumigatus lawns	Ag-in-alumina film	7.5	-	-
		28.5	fungistatic	19-24
		50	fungistatic	21-24
	$AgNO_3$	from 1 to 5 mg L^{-1}	fungicidic	1.5
G. candidum lawns	Ag-in-alumina film	7.5	-	-
		28.5	fungistatic	15-36
		50	fungistatic	21-25
	$AgNO_3$	from 1 to 5 mg L^{-1}	-	-

Table 2 The results of bacteria growth inhibition by various Ag-in alumina nanowire arrays and Ag+ ions.

Culture	Contacting materials	The content of Ag^o in μg or [Ag^+]	Effect	Zone of inhibition (in mm)
E. coli (-)	as-grown	7.5	-	-
	Ag-in-alumina film	28.5	bacteriocidic	3
		50	bacteriocidic	2-4
	$AgNO_3$	from 1 to 5 mg L^{-1}	-	-
M. luteus (+)	as grown	7.5	bacteriocidic	1.7
	Ag-in-alumina film	28.5	bacteriocidic	1.1-1.3
		50	bacteriocidic	1.5-1.7
	$AgNO_3$	from 1 to 5 mg L^{-1}	-	-